ehp Environmental Health PERSPECTIVES
ehponline.org
Published by the National Institute of Environmental Health Sciences

Uncoupling of ATP-mediated Calcium Signaling and Dysregulated IL-6 Secretion in Dendritic Cells by Nanomolar Thimerosal

Samuel R. Goth, Ruth A. Chu, Jeffrey P. Gregg, Gennady Cherednichenko, and Isaac N. Pessah

doi:10.1289/ehp.8881 (available at http://dx.doi.org/)
Online 21 March 2006

The National Institute of Environmental Health Sciences
National Institutes of Health
U.S. Department of Health and Human Services

Uncoupling of ATP-mediated Calcium Signaling and Dysregulated IL-6 Secretion in Dendritic Cells by Nanomolar Thimerosal

Samuel R. Goth[1,2]

Ruth A. Chu[2]

Jeffrey P. Gregg[1,3,4]

Gennady Cherednichenko[2]

Isaac N. Pessah[1,2,4]

[1]NIEHS Center for Children's Environmental Health, University of California at Davis, Davis California, USA

[2]Department of Veterinary Molecular Biosciences, University of California at Davis, Davis, California, USA

[3]Department of Medical Pathology, University of California at Davis, Davis, California, USA

[4]M.I.N.D. (Medical Investigation of Neurodevelopmental Disorders) Institute, University of California at Davis, Sacramento, California, USA

Corresponding Author: Isaac N. Pessah, Department of Veterinary Medicine: Molecular Biosciences, 1311 Haring Hall, One Shields Avenue, University of California, Davis, CA 95616. voice: (530) 752-6696, fax: (530) 752-4698. E-mail: inpessah@ucdavis.edu

Running Title Page

a) Running Title: Nanomolar thimerosal dysregulates DC signaling.

b) Keywords: Calcium, calcium channel, ethyl mercury, dendritic cell, immunotoxicity, interleukin-6, organic mercury, redox, thimerosal.

c) Acknowledgments, Grant Information: The authors acknowledge Christine Kwong for cytokine analyses. We thank Dr. Judy van de Water (Department of Medicine, Division of Rheumatology, Allergy and Clinical Medicine, UCD) for helpful discussions and for reviewing on the manuscript.

This work was supported by NIEHS Center for Children's Environmental Health (PO1 ES11269) and the M.I.N.D. Institute. Additional support came from the NIEHS Center for Environmental Health Sciences Cellular Imaging Core (ES05707). The authors declare they have no competing financial interests.

d) Abbreviations:

2-Me: 2-mercaptoethanol

7AAD: 7-aminoactinomycin D

Ca^{2+}: calcium

CICR: calcium-induced calcium release

DC: dendritic cell

DTaP: diptheria toxoid and acellular pertussis

ER/SR: endoplasmic reticulum/sarcoplasmic reticulum

EtHgCl: ethylmercuric chloride

FBS: fetal bovine serum

FSC: forward light scatter

HBSS: Hank's balanced saline solution

IDC: immature DC

IL-6: interleukin-6

IP_3R: inositol 1,4,5 trisphosphate receptor

JAK: janus kinase

MHC: major histocompatibility complex

MDC: mature DC

O_2: oxygen

PI: propidium iodide

rmGM-CSF: recombinant murine granulocyte-macrophage stimulating factor

Ry: ryanodine

RyR: ryanodine receptor

SOCC: store-operated Ca^{2+} channels

STAT: signal transducer and activator of transcription

TdT: terminal deoxynucleotidyl transferase

THI: thimerosal

TSA: thiosalicylic acid

ARTICLE DESCRIPTOR: Immune

Outline:

Abstract

Introduction

Materials and Methods

Results

Discussion

References

Table

Figure Legends

Figures

Abstract

Dendritic cells (DCs), a rare cell type widely distributed in the soma, are potent antigen presenting cells that initiate primary immune responses. DCs rely on intracellular redox state and calcium (Ca^{2+}) signals for proper development and function, but the relationship between these two signaling systems is unclear. Thimerosal (THI) is a mercurial used to preserve vaccines, consumer products, and experimentally to induce Ca^{2+} release from microsomal stores. We tested ATP-mediated Ca^{2+} responses of DCs transiently exposed to nanomolar THI. Transcriptional and immunocytochemical analyses show murine myeloid immature and mature DC (IDCs, MDCs) express inositol 1, 4, 5-trisphosphate and ryanodine receptor (IP_3R, RyR) Ca^{2+} channels, known targets of THI. IDCs express the RyR1 isoform in a punctate distribution that is densest near plasma membranes and within dendritic processes whereas IP_3Rs are more generally distributed. RyR1 positively and negatively regulates purinergic signaling since ryanodine (Ry) blockade (1) recruited 80 percent more ATP responders, (2) shortened ATP-mediated Ca^{2+} transients >2-fold, (3) and produced a delayed and persistent rise (≥2-fold) in baseline Ca^{2+}. THI (100nM, 5min) recruited more ATP responders, shortened the ATP-mediated Ca^{2+} transient (≥1.4-fold) and produced a delayed rise (≥3-fold) in the Ca^{2+} baseline, mimicking Ry. THI and Ry, in combination, produced additive effects leading to uncoupling of IP_3R and RyR1 signals. THI altered ATP-mediated IL-6 secretion, initially enhancing the rate of but suppressing overall cytokine secretion in DCs. DCs are exquisitely sensitive to THI, with one mechanism involving the uncoupling of positive and negative regulation of Ca^{2+} signals contributed by RyR1.

Introduction

Recent animal and human studies have underscored the strong influence of genetic, epigenetic, and physiological factors in defining susceptibility of the immune system to methyl mercury (MeHg) and ethyl mercury (EtHg) (Silbergeld et al. 2005; Havarinasab and Hultman 2005; Lawler et al. 2004). Immune dysregulation triggered by organic mercury can include suppression, stimulation, loss of tolerance and generation of autoantibodies. Therefore the pattern of immunotoxicity induced by organic mercury is likely to depend not only on the chemical form, timing and dose to which an individual is exposed but also to susceptibility factors that are poorly understood at present. Thus significant attention is currently focused on identifying which immune cell type(s) and biomolecules are critical targets of low-level organic mercury and their functional consequences on overall immune status.

Sodium ethylmercurithiosalicylate (thimerosal, THI) is an ethylmercury (EtHg)-containing compound used to preserve cosmetics, blood products and vaccines and is also used experimentally to induce calcium (Ca^{2+}) release from microsomal (ER/SR) stores in intact cells. THI toxicity is due to the EtHg moiety. THI and EtHg toxicity in humans comprise a few cases of accidental high dose poisoning (Cinca et al. 1980; Damluji, 1962; Zhang, 1984). Attention has been focused on THI in vaccines, where it is used as a preservative for multiuse formulations. THI was withdrawn from pediatric vaccines starting in 1999 (CDC, 1999) over concerns that organic mercury is a known neurodevelopmental toxicant. Nevertheless THI is still used in influenza, diptheria toxoid, DTaP, and tetanus toxoid vaccines. The hypothesis that THI can cause

neurodevelopmental disorders was tested by injecting THI and THI-containing vaccines into inbred strains of young mice (Hornig et al. 2004). Growth, behavioral, and histologic abnormalities in the brains of the autoimmune susceptible strain (SJL) were recorded after administration of THI or THI plus vaccine. Autoimmune-resistant strains (C57BL/6, BALB/c) did not display any of the abnormalities, suggesting a strong influence of inherent immune status and the neurodevelopmental toxicity of THI.

We hypothesized that an especially sensitive target of THI-mediated immune dysregulation are dendritic cells (DCs) whose function is to acquire antigens derived from self or nonself sources and efficiently present them to naïve and resting T cells (Banchereau and Steinman, 1998). This hypothesis stems from the fact that ambient oxygen (O_2) tension or thiol concentration directly influences DC secretion of IFN-γ and IL-12 (Murata et al. 2002), enhances expression of FcεR1 (Novak et al. 2002) and regulates surface class II major histocompatibility complex (MHC) expression (Goth et al. 2006) *in vitro*. In this regard, Ca^{2+} contributes essential signals for DC function and maturation. Differentiation (Bagley et al. 2004), proinflammatory cytokine secretion (Gardella et al. 2000), apoptotic cell phagocytosis (Poggi et al. 1998), and migrational responsiveness to purine nucleotides or chemokines (Partida-Sanchez et al. 2004; Scandella et al. 2004) are Ca^{2+}-dependent processes. DCs rely on changes in intracellular redox state and Ca^{2+} signals for proper development and function, but the relationship between these signaling systems in DC is unclear.

THI contains an oxidized mercury atom (Hg^{2+}) whose redox properties can enhance the activity of the inositol 1,4,5-trisphosphate (IP_3Rs) and ryanodine receptors (RyRs), both intracellular Ca^{2+} channels (Kaplin et al. 1994; Pessah et al. 2002). THI elicits Ca^{2+} release from endoplasmic/sarcoplasmic reticulum (ER/SR) stores in lymphocytes (Bultynck et al. 2004) and ER/SR microsomes by targeting the IP_3R and RyR (Abramson et al. 1995; Kaplin et al. 1994). THI-treated, monocyte-derived DCs failed to or minimally phosphorylated STAT proteins 1,3,4, and 6, implying the JAK signaling pathway, and by extension cytokine receptors, are bypassed in the sensitization phase induced by THI (Valk et al. 2002). DCs express several classes of Ca^{2+} channel proteins that mediate Ca^{2+} signals. DCs express store-operated Ca^{2+} channels (SOCC) (Hsu et al. 2001), and IP_3Rs that regulate release of Ca^{2+} from ER/SR stores in response to ATP (Schnurr et al. 2003) and chemokines (Scandella et al. 2004). Immature DC (IDCs) express message for one of three genetic forms of the RyR, the type 1 ryanodine receptor (RyR1) (Hsu et al. 2001; O'Connell et al. 2002). The influence of THI and its metabolites, ethylmercury and thiosalicylate, on Ca^{2+} signaling and activation of DCs remain unexplored.

To study how THI and EtHg influence Ca^{2+}-dependent DC functions we generated and tested murine DCs under normoxia (5% O_2 v/v) and omitted 2-mercaptoethanol (2-Me) from the culture medium. We report DCs primarily express the type 1 isoform of the IP_3R and RyR ER/SR Ca^{2+} channels, known targets of THI. THI and ryanodine each block early positive contributions of the RyR1 to ATP-induced Ca^{2+} transients and uncouple inhibitory feedback, indicating a common mechanism. The consequences of

THI upon ATP-induced IL-6 production, a Ca^{2+}-dependent process, were examined. THI initially enhanced the IL-6 secretion rate, but ultimately suppressed its accumulation. DCs are exquisitely sensitive to THI, with one prominent mechanism involving the uncoupling of positive and negative regulation of Ca^{2+} signals contributed by RyR1.

MATERIALS AND METHODS

Chemicals and Antibodies. THI (USP grade) and its metabolite thiosalicylic acid (TSA), propidium iodide (PI), diethylpyrocarbonate, and Na_2ATP were purchased from Sigma (St. Louis, MO). Fibronectin (bovine plasma) was purchased from Calbiochem (San Diego, CA). Ethylmercuric chloride (EtHgCl) was purchased from ICN (Costa Mesa, CA). Recombinant murine GM-CSF was purchased from Sigma or R&D Systems (Minneapolis, MN), as were murine IL-6 ELISA kits. Antibodies (BD-Pharmingen, San Diego, CA) are as follows with the clone name: class II MHC-biotin (2G9), CD11c-APC (HL3), CD16/32 (2.4G2), and hamster Ig. Anti RyR mAb 34C (recognizes types 1 and 3) was purchased from the Developmental Studies Hybridoma Bank (Iowa City, IA). Anti IP_3R and IP_3R1 pAbs were purchased from Chemicon (Temecula, CA). Prolong antifade, Fura-2 AM, Fluo-4AM, Alexa 488 conjugated goat anti mouse IgG and Alexa 488 conjugated goat anti rabbit IgG antibodies, and Alexa 647 conjugated goat anti rabbit IgG Ab were purchased from Invitrogen (Carlsbad, CA). 7-aminoactinomycin D (7AAD) was purchased from Calbiochem. A fluorescent terminal deoxynucleotidyl transferase (TdT) labeling kit was purchased from Promega (Madison, WI).

Cell Culture. Female C57BL/6J mice aged 6 to 8 weeks were purchased from JAX West, Inc. (Davis, CA) treated humanely and with regard of alleviation of suffering and euthanized in accordance with a protocol approved by the UC Davis Animal Resources Service. Bone marrow derived DCs were generated by modifying a protocol (Lutz et al. 1999), using normoxia (5% O_2 v/v) and omitting 50 μM 2-Me from the culture medium (Goth et al. 2006). R10 medium was RPMI 1640 (Invitrogen) with 10 percent fetal bovine serum (Hyclone, Logan, UT), 2 mM L-glutamine, 2 mM sodium pyruvate, and 100 IU/mL penicillin and 10 μg/mL streptomycin. Cultures were maintained at 37˚C in a Thermo Forma model 3130 incubator (Thermo Forma, Marietta, OH) equipped with a CO_2 and fuel-cell O_2 monitor and N_2 and CO_2 gas supplies. CO_2 was set to 5% v/v, O_2 to 5% v/v, and were periodically verified using Fyrite gas analyzers (Bacharach Inc, New Kensington, PA).

DC cytometric flow sorting and analysis. Cells were flow sorted between culture days 6 and 10. A detailed description of our cell preparation for flow cytometry has been published (Goth et al. 2006). Briefly, nonadherent cells were preblocked with 2.4G2 mAb (1.0 μg/ml) and hamster IgG (0.25 μg/ml) for 10 min. Fluorescent anti class II MHC (0.1 μg/ml) and anti CD11c (0.3 μg/ml) mAbs were added and allowed to bind for 15 min. After washing with 2 percent FBS (PBS:FBS), cells were aseptically sorted on a MoFlo cytometer (Cytometric, Fort Collins, CO). Single stained and unstained controls were used to define sorting gates and to adjust compensation. CD11c positive cells were considered DCs and graded as IDCs or MDCs depending on their class II MHC expression. We routinely obtained ≥85 percent purities of sorted IDC and MDC subsets.

Propidium iodide was added to a final concentration of 0.5 μg/mL before sorting or before analysis on a FACScan® flow cytometric analyzer (Becton Dickinson, Palo Alto, CA) to detect dead cells.

DC treatment. THI, EtHgCl, and TSA solutions were dissolved in sodium carbonate using borosilicate glass pipettes and tubes. Dilutions were made in R10 and used within 1 h. DCs (1-2x10^6 cells/ml) were aliquoted into perfluorocarbon tissue culture vials or 96 well format plates (Savillex, Minnetonka, MN). R10 or medium containing THI, EtHgCl, TSA, LPS (to 1 μg/ml) was added and cells placed in a 37˚C incubator.

DC transcriptome analysis. Total RNA was isolated as per the manufacturer's recommended procedure from sorted DCs using Trizol Reagent (Molecular Research Center, Cincinnati, OH). DCs were resuspended to 1x10^6 cell/ml in R10 media, plated in perfluorocarbon containers, and incubated for 20 h. Biotinylated cRNA was synthesized from 5 μg of total cellular RNA according to the protocol published by Affymetrix (Affymetrix Inc., Santa Clara, CA). Fragmented, labeled cRNA was hybridized onto Affymetrix mouse 430A or 430 2.0 GeneChip arrays (Affymetrix Inc.). Microarrays were hybridized 16 h at 45°C, stained and washed according to an Affymetrix protocol (EukGE-WS2v4). Fluorescence intensity was measured with a scanner equipped with Affymetrix Microarray Analysis Suite version 5.0 (MAS 5.0). The average intensity for each array was normalized by scaling to a target intensity value of 125 allowing comparison between arrays. Individual transcripts are represented by perfect match

probes in conjunction with a corresponding set of mismatch probes. A transcript is called present if the average intensity value of perfect match cells is ≥ 1.5 times greater than the average intensity of mismatch cells, and the average intensity difference between perfect match and mismatch cells is ≥ four times the experimental noise. Poorly performing probes (where the ratio between the average intensity of mismatch cells and perfect match cells is ≥ four times the experimental noise) were not included in the analysis. RNA from 3 independent cultures was analyzed on GeneChips (*i.e.*, 3 GeneChips per treatment were analyzed).

Immunocytofluorescence of calcium channels. DCs were washed in 1% BSA:PBS, centrifuged onto glass slides using a Cytofuge2 (Statspin, Norwood, MA), air dried, fixed with 4% paraformaldehyde:PBS for 20 min at 4°C, then permeabilized with three washes of 0.2% Tween-20 in PBS (TPBS). Nonspecific binding was blocked with goat IgG (50 μg/mL). Cells were incubated with primary Ab (dilutions were 1:20 34C; 1:100 anti-IP_3R and IP_3R1 pAbs in TPBS) for 1 h. Blocking peptide for the IP_3R1 Ab was used at the manufacturer's suggested concentration. After washing Alexa 488 or Alexa 647 conjugated anti -mouse and anti- rabbit secondary Ab were diluted 1:1000 in TPBS and allowed to bind 1 h. Cells were washed with TPBS, then with PBS. After mounting with Prolong antifade plus 40 μg/ml 7AAD, DCs were visualized for immunofluorescence using a Bio-Rad MRC 600 laser scanning confocal microscope (Richmond, CA). Confocal immunophenotyping was performed on two separate cultures.

Terminal deoxynucleotidyl transferase (TdT) assay. IDCs were treated with 500 nM TSA, THI or medium for 20 h as described above. Cells were then washed twice with ice cold PBS, then fixed with 4% paraformaldehyde:PBS for 20 min on ice. Cells were washed in PBS:1% BSA, resuspended to $0.5x10^6$ cells/mL in PBS:1% BSA, and cell aliquots spun onto microscope slides. Slides were air dried at least 2 hours, then immersed in 4% diethylpyrocarbonate:EtOH prechilled to -20 degrees for 30 min to stop endogenous nuclease activity. After washing twice with PBS cells were processed for DNA strand-end labeling according to the protocol supplied by the kit manufacturer. After TdT labeling nuclei were counterstained with 1 µg/mL PI in water for 15 minutes before mounting in Prolong antifade for confocal imaging.

[^{3}H]Ryanodine binding analysis. High affinity binding of [^{3}H]ryanodine ([^{3}H]Ry; 56 or 50 Ci/mmol, Perkin-Elmer, Boston, MA) to rabbit skeletal microsomes enriched in RyR1 was performed as previously described (Pessah et al. 1987). Nonspecific binding was determined by including 1000-fold unlabelled ryanodine. Data was reported in pmole bound Ry/mg protein.

IL-6 assays. IDCs were pulsed with 100 nM THI or TSA for 20 min, pelleted, supernatant aspirated, and resuspended to $2x10^7$/ml. 0.05 ml of the cell suspension was aliquoted per well into a perfluorocarbon 96 well plate and 0.05 ml ATP (0, 0.2, 2 or 20 µM final) added per well. Medium and LPS (1 µg/mL final) cells received no pretreatment. Supernatants for IL-6 ELISA were collected 20 h later from the top portion

of the cultures. IL-6 concentrations were interpolated from the linear response range of the cytokine standard, minimum sensitivity was 7 pg/ml.

Calcium imaging. IDCs were resuspended in R10 supplemented with 5 ng/mL rmGM-CSF to $0.5x10^6$/ml. 0.5 ml was plated overnight onto fibronectin coated glass coverslips. The next day, cells were labeled with 5 μM fura-2AM or fluo-4AM for 20 min. Cells were washed with bathing solution (in mM): 130 NaCl, 4 KCl, 10 Hepes, 10 glucose, 2 $CaCl_2$, 2 $MgSO_4$, pH 7.3 (with NaOH) and imaged within 1 h. Changes in cytoplasmic Ca^{2+} were measured by emission at 510 nm (fluo-4) or ratioing emission at 510nm with excitation pair 340/380 nm (fura-2) (Fessenden et al. 2003). Rapid perfusion of ATP and caffeine was accomplished by a micropipette above the cells being imaged (Automate, Oakland CA).

Data analysis. Non-linear curve fitting analysis and one-way ANOVA were performed using Origin 6.0 (Northampton, MA) software to test for statistical significance.

RESULTS

Culturing murine bone marrow at physiologic O_2 tension (5% v/v) without 2-mercaptoethanol (2-Me) supplementation generated myeloid IDCs and MDCs with a similar yield, leukocyte marker expression, and allostimulatory capacity as DC produced from cultures using ambient (20%) O_2 and 50 μM 2-Me (Goth et al. 2006). A representative flow cytometric dot-plot showing sorting gates for IDC and MDC is shown

in Supplemental Figure 1A. RNAs extracted from sorted IDCs and MDCs were analyzed using gene probe arrays. IDCs and MDCs have a common lineage, and a small number of changes in gene expression occurred during maturation. Of this limited set of genes, class II MHC mRNA expression is down regulated with maturation, whereas *CD86* message was upregulated with maturation (Table 1). *GADPH* was expressed at similar levels in IDCs and MDCs (Table 1). Both DC subsets express two Ca^{2+} channel types that are targets of THI. Of the 3 IP_3R isoforms, IDCs and MDCs express message for *ITPR1* and *ITPR3*, the latter downregulated with maturation (Table 1). Of the 3 RyR isoforms, *RyR1* mRNA is present in both DC subsets, *RyR3* is expressed upon maturation and *RyR2* is not expressed (Table 1). As the Ca^{2+} channel genes detected encode targets of THI (see below) we explored the distribution of the proteins in IDCs using confocal microscopy.

IDCs express IP_3R1 in a dense granular distribution in a pattern consistent with targeting to ER membranes (Figures 1A and E). In contrast, intense RyR1 staining localizes near the plasma membrane, and foci of protein extend from the base into dendrites (Figures 1C, E, and F). IDCs lack detectable RyR1 within perinuclear regions (Figures 1C, E, and F). Cells stained with secondary Ab alone or with Ab-blocking peptide (IP_3R1) had no detectable signal (Figures 1B and D). The co-distribution of RyR1 and IP_3R was further examined using an anti-RyR1 mAb and a pan anti-IP_3R polyclonal Ab. The RyR1 is densely localized within a narrow band at the cell periphery and extends within dendrites (Figures 1E and F), whereas IP_3R extends to regions lacking RyR1 (Figure 1E). The granular appearance and distribution of IP_3R protein in IDCs did not change when visualized with an isoform specific (IP_3R1) or pan-IP_3R Ab (Figures 1 A

and E). The distribution of RyR proteins in IDCs and MDCs (using a mAb specific for RyR1 and 3) were similar (Figures 1G and H) despite the additional expression of *RyR3* transcripts in MDC (Table 1).

Ca^{2+} responses of IDCs to the RyR agonist caffeine were tested. Given the expression of RyR1 within IDCs, and that MDCs respond to caffeine (Schnurr et al. 2003), we expected IDCs would respond to caffeine with a rise in cytoplasmic Ca^{2+}. Approximately 50% of IDCs responded to 20 mM caffeine (Figure 2A). Since extracellular ATP induces maturity in IDCs (la Sala et al. 2001, la Sala et al. 2002; Schnurr et al. 2001) and intracellular Ca^{2+} contributes an essential DC maturation signal (Bagley et al. 2004), we decided to test the ability of our IDCs to respond to extracellular ATP. IDCs responded vigorously to a brief (5 s) application of ATP, the response amplitude dose-dependent between 0.2 and 20 μM (Figure 2B). Therefore ATP potently elicits Ca^{2+} transients, likely mediated through agonist actions on P2Y purinergic nucleotide receptors expressed in IDCs (Idzko et al. 1999). We next generated viability-dose survival curves for DCs exposed to THI and its metabolites ethylmercury (from ethylmercuric chloride, EtHgCl) and thiosalicylic acid (TSA; chemical structures are shown in Supplemental Figure 1B).

Range-finding experiments determined that a 20 h exposure to 10 μM THI consistently killed >90% of DCs using flow cytometry, judged by their increased permeability to propidium iodide (PI) and decreased cell size (forward light scatter, FSC; data not shown). THI, EtHgCl, and TSA were titrated from 50 nM to 10 μM, IDC and MDC subsets treated for 20 h, and cell PI permeability measured by flow cytometry.

Figures 3A and B show THI and EtHgCl caused dose-dependent decreases in DC viability compared to the TSA control. The viability dose response curves for THI and EtHgCl were the same within each DC subset, and were similar between the cell subsets. IC_{50} values for the DC subsets treated with THI, TSA, and EtHgCl are shown in Figures 3A and B. DC death triggered by THI could be mediated by apoptosis or primary necrosis, as the FSC and PI uptake data acquired 20 h post-treatment cannot distinguish between the two possibilities. IDC were treated with medium alone, 500 nM TSA, or 500 nM THI for 20 h and probed for DNA strand breakage, an indicator of apoptosis (Figures 3C, D and E, respectively). Only THI treated cells demonstrate both increased dUTP-FITC labeling and a corresponding shrinkage in nuclear size (Figure 3E); death from THI exposure is therefore likely to be an apoptotic outcome. The action of THI and EtHgCl upon RyR1 channels was further explored by measuring [^{3}H]Ry binding to ER/SR membranes enriched in RyR1. THI and EtHgCl inhibited the specific binding of [^{3}H]Ry to RyR1 (Figure 3F, IC_{50}=562 and 501 nM).

Lymphocyte tolerance or immunity to an antigen can be driven by immature or mature DC respectively (Steinman et al. 2005) and we focused on characterizing the effects of THI upon ATP-mediated Ca^{2+} signaling (a maturation signal) in IDCs. THI can release Ca^{2+} from ER/SR stores by selectively enhancing the activity of IP_3R and RyR, and we examined its actions on ATP-mediated Ca^{2+} signaling in IDC. ATP is an efficacious activator of DC through its agonist actions on P2Y purinergic nucleotide receptors (Idzko et al. 2002). P2Y receptors couple to Gαq protein that initiates signal transduction events leading to the hydrolysis of phosphatidylinositol 4,5-bisphosphate

(PIP_2) to IP_3 and diacylglycerol. IP_3 in turn activates IP_3R that mobilizes Ca^{2+} from ER stores (Di Virgilio et al. 2001a; Di Virgilio et al. 2001b). IDC challenged with two pulses of 20 μM ATP (5 s each) 30 min apart (with constant perfusion) produced Ca^{2+} transients whose peak heights, baseline to peak rates or peak to baseline decays, were not significantly different (Figure 4, top trace). This indicates that the concentration, duration, and frequency of the ATP challenges did not desensitize the cell's capacity to respond nor were they additive.

Perfusion of 50 nM THI after an initial ATP test pulse (Figure 4, middle trace) did not induce a rise in baseline Ca^{2+} in the 30 min of perfusion that preceded the second ATP challenge. In the presence of THI, the second ATP pulse produced a baseline to Ca^{2+} peak height comparable to that elicited by the first ATP challenge. However the rate of decay of the response peak was significantly slowed by THI compared to control cells. THI also induced a sustained elevation in the 8 min of trace recording in intracellular Ca^{2+} after ATP withdrawal. DC exposed to 100 nM THI (Figure 4, lower trace) showed a gradual rise in resting Ca^{2+}. Although cells responded to a second ATP challenge, decay of the response was significantly slower and incomplete compared to DC exposed to 50 nM THI. Following withdrawal of ATP from the perfusion medium, a more pronounced slow rise of intracellular Ca^{2+} concentration was seen and remained elevated for the duration of the measurement. Some DC tested with 20 μM ATP failed to show detectable responses. However these 'ATP resistant' cells invariably responded vigorously to ATP after exposure to 50 nM THI for 30 min (not shown). We next dissected the ATP-

mediated calcium wave in DCs using pharmacological agents known to modify components of Ca^{2+} signaling.

ATP generated a stereotyped Ca^{2+} transient having a time to peak of 16.1±2.6 s and a decay time of 106±2.6 s (Figure 5A first trace from top). To test the RyR1s contribution to ATP-mediated Ca^{2+} transients, IDCs were pretreated 4 h with 100 μM ryanodine (Ry), which irreversibly locks the RyR in a non-conducting conformation (Buck et al. 1999; Zimanyi et al. 1992). ATP challenged Ry-treated cells produced transients whose time to peak did not significantly differ from control (Figure 5A, second trace, and Figure 5B). However, after ATP withdrawal, the recovery time to baseline was >2-fold (p <0.01) faster (Figures 5A, second trace, and Figure 5C) and showed a delayed and persistent rise (p =0.036) in baseline Ca^{2+} after triggering (Figures 5A, second trace, and Figure 5D). A 5 min THI (100 nM) pre-exposure mimicked the effects of Ry. When challenged with ATP, the rise time remained unchanged (Figure 5B), but the Ca^{2+} transient was shortened >1.5-fold (p =0.05; Figure 5C) and the delayed rise in Ca^{2+} baseline was prominent (p =0.02) (Figures 5A, third trace, and Figure 5D).

The effects of THI and Ry in combination were nearly additive (Figure 5A, fourth trace, Figures 5C and D), suggesting a common mechanism targeting RyR1 function. THI and Ry alone or combined increased the number of IDCs responding to ATP 1.5 to 1.8 fold compared to control (p <0.05; Figure 5E). THI's actions on IDC Ca^{2+} signaling were not seen with TSA, therefore they were mediated by organic mercury (not shown). These results (Figures 4 and 5) identify that as little as 50-100 nM THI in the span of a

few minutes (5-30) potentiates agonist mediated Ca^{2+} signaling events in DC that primarily manifest as a prolonged elevation in intracellular Ca^{2+}. DC are arguably the most sensitive target cell for THI identified to date, and this sensitivity to oxidative insult may reflect a unique manner in which they generate and utilize Ca^{2+} signals in response to a changing redox environment.

Increased intracellular Ca^{2+} induced by inhibitors of the SR/ER Ca^{2+}-ATPase is associated with the rapid secretion of macrophage IL-6 (Bost and Mason 1995). DCs produce IL-6 in response to IL-1β, TNF-α or LPS, and other myeloid cells secrete IL-6 in response to ATP (Shigemoto-Mogami et al. 2001). We hypothesized that THI-induced uncoupling of ATP-mediated Ca^{2+} signaling would disrupt IL-6 secretion. IDCs were pretreated with 100 nM THI or TSA, challenged with graded concentrations of ATP, and secreted IL-6 measured. In Figure 6A, IDCs pretreated with THI or TSA alone secreted low levels of IL-6 that did not significantly differ from the medium control. LPS, which induces IL-6 synthesis by non-Ca^{2+} dependent pathways, induced a large increase in IL-6. All three ATP concentrations induced comparable amounts of IL-6 by the TSA-pretreated DCs. By 20 h, these IL-6 concentrations were equal to the LPS treated control. Pretreating IDCs with THI and challenging with ATP attenuated IL-6 secretion compared to TSA-pretreated controls, reaching significance at the lowest (0.2 μM) ATP dose. This lowered IL-6 secretion was not due to cell death as this was overcome by 2 and 20 μM ATP. Next we determined the kinetics of ATP-mediated IL-6 secretion in THI-treated DC to see if cytokine production was attenuated at earlier time points.

In Figure 6B, 2 μM ATP induced IL-6 by 4 h, consistent with its rapid induction in other myeloid cells. THI pretreatment accelerated IL-6 secretion compared to TSA controls, indicating THI sensitized DC to ATP. Maximal IL-6 was secreted by THI-treated DC by 8 h where controls needed an additional 12 h. 20 μM ATP was more potent than 2 μM, eliciting IL-6 by 2 h and near-maximal levels at 8 h in both THI- and TSA-pretreated control IDCs (Figure 6C). The strong accelerating effect of THI *vs.* TSA on IL-6 secretion induced by 2 μM ATP was not as pronounced with 20 μM ATP, generating a small but significant increase 4 h after its application (Figure 6C).

DISCUSSION

DC activation and associated immune functions are subject to regulation by their redox environment (Bagley et al. 2004; Gardella et al. 2000; Goth et al. 2006; Murata et al. 2002; Novak et al. 2002). We generated DC under tightly regulated O_2 and without 2-Me to provide a more physiologic baseline to study the mechanism of redox active environmental triggers such as THI and EtHg in regulating DC activation *in vitro*. For DCs, Ca^{2+} signaling events provide an essential 'upstream' component, engaging immediate events such as cytokine production and secretion (Ferrari et al. 2000; la Sala et al. 2002) and long-term (*e.g.,* maturational) responses. Importantly, microsomal IP_3R and RyR Ca^{2+} channel functions are tightly regulated by changes in local redox state (Bultynck et al. 2004; Kaplin et al. 1994; Pessah et al. 2002).

We show for the first time the expression and distribution of two major Ca^{2+} channel proteins expressed in DCs. We have provided transcriptomal and direct

immunocytochemical evidence that DCs express specific isoforms of the IP_3R and RyR Ca^{2+} channels. RyR and IP_3R proteins distinctly distribute in DC subsets. In IDCs, the RyR1 and IP_3R1 localize below the plasma membrane at the base of the dendrites and into the processes. A similar distribution of the RyR was seen in MDCs. However IP_3Rs extend to reticular regions where the RyR1 is either absent or at very low levels. In human monocytes, IP_3R and RyR localization patterns similar to our murine DCs were found (Clark and Petty 2005).

ATP-triggered Ca^{2+} transients in IDCs have 3 components that engage cross-talk between IP_3Rs and RyRs. The initial rate and amplitude of the Ca^{2+} transient (Phase 1; Figure 7) is largely dependent upon IP_3R activation. It is unlikely the RyR1 has a significant influence on Phase 1 since blocking RyR1 channels with Ry has no measurable consequence on these parameters. The transient decay rate depends on both IP_3R and RyR1, since blocking RyR1 channels with Ry significantly enhances this rate back to baseline (Phase 2; Figure 7). Ca^{2+}-induced Ca^{2+} release, presumably mediated by activation of RyR1, must therefore contribute to slowing the decay rate.

However RyR1 activity in IDCs also contributes to the negative regulation re-establishing a stable resting Ca^{2+} level to near that before activation of purinergic signaling (Phase 3; Figure 7). Phase 3 was unmasked when Ry or THI modified RyR1 conformation. Phase 2 and 3 are coupled events that rely on the conformational state of the RyR1. In this regard, both micromolar Ry and nanomolar THI uncouple functional

cross-talk between IP_3R and RyR1 channels normally regulating purinergic signaling in IDCs.

Collectively these data show RyR1 channels are closely coupled to IP_3-induced Ca^{2+} release, and contribute to the temporal properties of the transient by (1) prolonging the decay and (2) restoring the original resting Ca^{2+} level. RyR1 therefore contributes both positive and negative regulation to purinergic signaling in IDCs. THI, like Ry, appears to uncouple RyR1 functions from phosphoinositide signaling in IDCs in a concentration and time dependent manner.

Nanomolar THI deregulated ATP mediated signaling by a mechanism that uncoupled Phase 2 and 3 of the Ca^{2+} transient. THI did not appear to influence the initial response to ATP by activation of the IP_3R (Phase 1), but enhanced the transient decay rate after agonist withdrawal (Phase 2) and elicited a persistent rise in intracellular Ca^{2+} (Phase 3). THI's actions on IP_3R mediated signals have not been previously explored in DCs. However evidence indicates the IP_3R1 is a target of THI. Using triple IP_3R-knockout R23-11 cells derived from DT40 chicken B lymphoma cells, THI (1-100 nM) potentiated IP_3-induced Ca^{2+} release when IP_3R1, but not IP_3R3, is expressed (Bultynck et al. 2004).

RyR1 is also a sensitive target of THI (Figure 3E present study; Abramson et al. 1995). We show ATP triggers a Ca^{2+} transient in IDCs whose temporal property relies on functional coupling of IP_3R and RyR1 channels that is extremely sensitive to THI ($\leq$100

nM). How THI sensitizes RyR1 to activation by Ca^{2+} involves release of the inhibitory actions of Mg^{2+}, an important physiological modulator (Donoso et al. 2000; Sanchez et al. 2003) and may be mediated by hyperreactive cysteines within the RyR1 channel complex (Liu and Pessah 1994; Voss et al. 2004). Exactly how THI alters ATP-dependent and independent Ca^{2+} signals may involve multiple molecular mechanisms involving the IP_3R1, RyR1, and possibly other channels. Nevertheless the present results reveal that IDCs are a particularly sensitive target of THI, with as little as 50 nM within 30 min uncoupling ATP-induced Ca^{2+} transients.

DC sensitivity to their oxidative environment may reflect how they generate and utilize Ca^{2+} signals in response to a changing redox environment. Redox modulation of DC function is underscored by our finding that THI modulates IL-6 synthesis elicited by exogenous ATP. Myeloid DC IL-6 strongly influences mucosal T cell and gut B cell responses. Lung DCs with intrinsic Th2 polarizing activities generated Th1 responses from naïve CD4+ T cells in the presence of anti-IL-6 neutralizing Ab (Dodge et al. 2003). Peyer's patch B cells were induced to secrete IgA by IL-6 elaborated by local $CD11b^+$ DC; IgA induction was reduced by anti-IL-6 Abs (Sato et al. 2003).

In vivo ATP steady state levels are at nanomolar and low micromolar (1-25 μM) concentrations in bulk fluids and at the cell surface respectively (Lazarowski et al. 2003). At these concentrations, metabotropic G-protein coupled P2Y receptors are engaged. In THI-treated DCs IL-6 production kinetics are enhanced by 2 μM and 20 μM ATP, and IL-6 secretion is significantly suppressed by 0.2 μM ATP (Figure 6A). THI-enhanced IL-

6 secretion may be a consequence of prolonged calcium signals resulting from the uncoupling effects of THI toward IP_3R and RyR1 mediated signals. Increased intracellular Ca^{2+} is associated with IL-6 RNA stabilization and rapid IL-6 secretion (Bost and Mason 1995). THI-mediated attenuation of IL-6 secretion at 0.2 μM ATP was not unexpected as the suboptimal calcium signals induced by 0.2 μM ATP may have not been sufficient to promote maximal rates of IL-6 synthesis. Ca^{2+} stimulated RyR1 channels are initially activated and then inactivated by THI (Figure 3F this study; Abramson et al. 1995). Over the 20 h assay used in this study, the uncoupling of IP_3R-RyR1 functions are likely to have broad effects upon Ca^{2+} dependent processes.

A practical implication of the present findings has relevance to the commercial uses of THI as an antimicrobial agent in vaccines and consumer products since they identify DC as sensitive targets for THI and ethylmercury mediated dysfunction. Given the importance of DC as a front line in regulating lymphocyte mediated immunity and tolerance, altering DC functions by forms of ethylmercury should be considered when assessing contributions to altered immune function. In studies using autoimmune-susceptible A.SW ($H\text{-}2^s$) mouse strain, THI induces a syndrome that is stronger and more generally manifested than those produced by methylmercury (Havarinasab et al. 2004) and development of autoimmunity in $H\text{-}2^s$ mice is dependent on cellular (T cell) and soluble (IFN-γ and IL-6) factors (Havarinasab et al. 2005). Onset of spontaneous systemic autoimmune disease symptoms (proteinuria, anti-DNA antibodies) in (NZBxNZW)F1 mice is hastened by THI (Havarinasab et al. 2006). Interestingly, disease morbidity and mortality in these F1 mice is dramatically reduced by neutralizing anti-IL-

6 receptor antibody (Mihara et al. 1998), an effect associated with reduced IgG (auto-) antibody production.

The human *RyR1* gene is highly polymorphic. Over 60 single missense/deletional mutations have been closely linked to the pharmacogenetic disorders malignant hyperthermia and central core disease (Gronert et al. 2004). Our findings that DCs primarily express the RyR1 channel complex, and that uncoupling of this complex by very low levels of THI with dysregulated IL-6 secretion, raises intriguing questions about a molecular basis for immune dyregulation and the possible role of the RyR1 complex in genetic susceptibility of the immune system to mercury.

REFERENCES

Abramson JJ, Zable AC, Favero TG, Salama, G. 1995. Thimerosal interacts with the Ca2+ release channel ryanodine receptor from skeletal muscle sarcoplasmic reticulum. J Biol Chem 270:29644-29647.

Bagley KC, Abdelwahab SF, Tuskan RG, Lewis GK. 2004. Calcium signaling through phospholipase C activates dendritic cells to mature and is necessary for the activation and maturation of dendritic cells induced by diverse agonists. Clin Diagn Lab Immunol 11: 77-82.

Banchereau J, Steinman RM. 1998. Dendritic cells and the control of immunity. Nature 392: 245-252.

Bost KL, Mason MJ. 1995. Thapsigargin and cyclopiazonic acid initiate rapid and dramatic increases of IL-6 mRNA expression and IL-6 secretion in murine peritoneal macrophages. J Immunol 155:285-296.

Buck D, Zimanyi I, Abramson JJ, Pessah IN. 1992. Ryanodine stabilizes multiple conformational states of the skeletal muscle calcium release channel. J Biol Chem 267:23560-23567.

Bultynck G, Szlufcik K, Nadif Kasri N, Assefa Z, Callewaert G, Missiaen L, et al. 2004. Thimerosal stimulates Ca 2+ flux through inositol 1,4,5-trisphosphate receptor type 1 but not type 3 via modulation of an isoform-specific Ca 2+-dependent intramolecular interaction. Biochem J 381:87-96.

CDC. 1999. Notice to Readers: Thimerosal in vaccines: A joint statement of the American Academy of Pediatrics and the Public Health Service. MMWR 48:563-565.

Cinca I, Dumitrescu I, Onaca P, Serbanescu A, Nestorescu B. 1980. Accidental ethyl mercury poisoning with nervous system, skeletal muscle, and myocardium injury. J Neurol Nerosurg Psychiatry 43:143-149.

Clark AJ, Petty HR. 2005. Differential intracellular distributions of inositol trisphosphate and ryanodine receptors within and among hematopoietic cells. J Histochem Cytochem 53: 913-916.

Damluji S. 1962. Mercurial poisoning with the fungicide Granosan. M .J. Fac. Med. (Baghdad) 4:83-103.

Dodge IL, Carr MW, Cernadas M, Brenner MB. 2003. IL-6 production by pulmonary dendritic cells impedes Th1 immune responses. J Immunol 170:4457-4464.

Donoso P, Aracena P, Hidalgo C. 2000. Sulfhydryl oxidation overrides Mg(2+) inhibition of Ca2+ -induced Ca2+ release in skeletal muscle triads. Biophys J 79:279-286.

Elferink JG, de Koster BM. 1998. The effect of thimerosal on neutrophil migration: a comparison with the effect on Ca2+ mobilization and CD11b expression. Biochem Pharmacol 55:305-312.

Ferrari D, La Sala A, Chiozzi P, Morelli A, Falzoni S, Girolomoni G, et al. 2000. The P2 purinergic receptors of human dendritic cells: identification and coupling to cytokine release. Faseb J 14:2466-2476.

Fessenden JD, Perez CF, Goth S, Pessah IN, Allen PD. 2003. Identification of a key determinant of ryanodine receptor type 1 required for activation by 4-chloro-*m*-cresol. J Biol Chem 278:28727-28735.

Gardella S, Andrei C, Poggi A, Zocchi MR, Rubartelli A. 2000. Control of interleukin-18 secretion by dendritic cells: role of calcium influxes. FEBS Lett 481:245-248.

Gomez MF, Stevenson AS, Bonev AD, Hill-Eubanks DC, Nelson MT. 2002. Opposing actions of inositol 1,4,5-trisphosphate and ryanodine receptors on nuclear factor of activated T-cells regulation in smooth muscle. J Biol Chem 277:37756-37764.

Goth SR, Chu RA, Pessah IN. 2006. Oxygen tension regulates the *in vitro* maturation of GM-CSF expanded murine bone marrow dendritic cells by modulating class II MHC expression. J Immunol Methods 308:179-91.

Gronert, G. A., Pessah, I. N., Muldoon, S. M., and Tautz, T. J. (2004) Malignant Hyperthermia. In Anesthesia, 6th Edition, Miller, RD, ed., pp1033-1052, Churchill Livingstone, Phil. PA.

Haak LL, Song LS, Molinski TF, Pessah IN, Cheng H, Russell JT. 2001. Sparks and puffs in oligodendrocyte progenitors: cross talk between ryanodine receptors and inositol trisphosphate receptors. J Neurosci 21:3860-3870.

Havarinasab S, Lambertsson L, Qvarnstrom J, Hultman P. 2004. Dose-response study of thimerosal-induced murine systemic autoimmunity. Toxicol Appl Pharmacol 194:169-179.

Havarinasab S, Hultman P. 2005. Organic mercury compounds and autoimmunity. Autoimmun Rev 4:270-275.

Havarinasab S, Haggqvist B, Bjorn B, Pollard KM, Hultman P. 2005. Immunosuppressive and autoimmune effects of thimerosal in mice. Toxicol Appl Pharmacol 204:109-121.

Havarinasab S, Hultman P. 2006. Alteration of the spontaneous systemic autoimmune disease in (NZBxNZW)F1 mice by treatment with thimerosal ethyl mercury). Toxicol Appl Pharmacol article in press.

Hornig M, Chian D, Lipkin WL. 2004. Neurotoxic effects of postnatal thimerosal are mouse strain dependent. Mol Psychiatry 9:833-845.

Hsu S, O'Connell PJ, Klyachko VA, Badminton MN, Thomson AW, Jackson MB, et al. 2001. Fundamental Ca2+ signaling mechanisms in mouse dendritic cells: CRAC is the major Ca2+ entry pathway. J Immunol 166:6126-6133.

Idzko M, Dichmann S, Ferrari D, Di Virgilio F, la Sala A, Girolomoni G, et al. 2002. Nucleotides induce chemotaxis and actin polymerization in immature but not mature human dendritic cells via activation of pertussis toxin-sensitive P2y receptors. Blood 100:925-932.

InSug O, Datar S, Koch CJ, Shapiro IM, Shenker BJ. 1997. Mercuric compounds inhibit human monocyte function by inducing apoptosis: evidence for formation of reactive

oxygen species, development of mitochondrial membrane permeability transition and loss of reductive reserve. Toxicology 124:211-224.

Kaplin AI, Ferris CD, Voglmaier SM, Snyder SH. 1994. Purified reconstituted inositol 1,4,5-trisphosphate receptors. Thiol reagents act directly on receptor protein. J Biol Chem 269:28972-28978.

Korkotian E, M Segal. 1999. Release of Ca^{2+} from stores alters the morphology of dendritic spines in cultured hippocampal neurons. Proc Natl Acad Sci U S A 96:12068-12072.

la Sala A, Ferrari D, Corinti S, Cavani A, Di Virgilio F, Girolomoni G. 2001. Extracellular ATP induces a distorted maturation of dendritic cells and inhibits their capacity to initiate Th1 responses. J Immunol 166:1611-1617.

la Sala A, Sebastiani S, Ferrari D, Di Virgilio F, Idzko M, Norgauer J, et al. 2002. Dendritic cells exposed to extracellular adenosine trisphosphate acquire the migratory properties of mature cells and show a reduced capacity to attract type 1 T lymphocytes. Blood 99:1715-1722.

Lawler CP, Croen LA, Grether JK, Van de Water J. 2004. Identifying environmental contributions to autism: provocative clues and false leads. Ment Retard Dev Disabil Res Rev 10:292-302.

Lazarowski ER, Boucher RC, Harden TK. 2003. Mechanism of release of nucleotides and integration of their action as P2X- and P2Y-receptor activating molecules. Mol Pharmacol 64:785-795.

Liu G, Pessah IN. 1994. Molecular interaction between ryanodine receptor and glycoprotein triadin involves redox cycling of functionally important hyperreactive sulfhydryls. J Biol Chem 269:33028-33034.

Lutz MB, Kukutsch N, Ogilvie AL, Rossner S, Koch F, Romani N, et al. 1999. An advanced culture method for generating large quantities of highly pure dendritic cells from mouse bone marrow. J Immunol Methods 223:77-92.

McGeown JG. 2004. Interactions between inositol 1,4,5-trisphosphate receptors and ryanodine receptors in smooth muscle: one store or two? Cell Calcium 35:613-619.

Mihara M, Takagi N, Takeda Y, Ohsugi Y. 1998. Il-6 receptor blockade inhibits the onset of autoimmune kidney disease in NZB/W F1 mice. Clin Exp Immunol 112:397-402.

Morales-Tlalpan V, Arellano RO, Diaz-Munoz M. 2005. Interplay between ryanodine and IP3 receptors in ATP-stimulated mouse luteinized-granulosa cells. Cell Calcium 37:203-213.

Murata Y, Ohteki T, Koyasu S, Hamuro J. 2002. IFN-gamma and pro-inflammatory cytokine production by antigen-presenting cells is dictated by intracellular thiol redox status regulated by oxygen tension. Eur J Immunol 32:2866-2873.

Novak N, Kraft S, Haberstok J, Geiger E, Allam P, Bieber T. 2002. A reducing microenvironment leads to the generation of FcepsilonRIhigh inflammatory dendritic epidermal cells (IDEC). J Invest Dermatol 119:842-849.

O'Connell PJ, Klyachko VA, Ahern GP. 2002. Identification of functional type 1 ryanodine receptors in mouse dendritic cells. FEBS Lett 512:67-70.

Ooashi N, Futatsugi A, Yoshihara F, Mikoshiba K, Kamiguchi H. 2005. Cell adhesion molecules regulate Ca^{2+}-mediated steering of growth cones via cyclic AMP and ryanodine receptor type 3. J Cell Biol 170:1159-1167.

Partida-Sanchez S, Goodrich S, Kusser K, Oppenheimer N, Randall TD, Lund FE. 2004. Regulation of dendritic cell trafficking by the ADP-ribosyl cyclase CD38: impact on the development of humoral immunity. Immunity 20:279-291.

Pessah IN, Stambuk RA, Casida JE. 1987. Ca^{2+}-activated ryanodine binding: mechanisms of sensitivity and intensity modulation by Mg^{2+}, caffeine, and adenine nucleotides. Mol Pharmacol 31:232-238.

Pessah IN, Kim KH, Feng W. 2002. Redox sensing properties of the ryanodine receptor complex. Front Biosci 7a:72-79.

Poggi A, Rubartelli A, Zocchi MR. 1998. Involvement of dihydropyridine-sensitive calcium channels in human dendritic cell function. Competition by HIV-1 Tat. J Biol Chem 273:7205-7209.

Sanchez G, Hidalgo C, Donoso P. 2003. Kinetic studies of Ca^{2+} -induced Ca^{2+} release in cardiac sarcoplasmic reticulum vesicles. Biophys J 84:2319-2330.

Sato A, Hashiguchi M, Toda E, Iwasaki A, Hachimura S, Kaminogawa S. 2003. CD11b+ Peyer's patch dendritic cells secrete IL-6 and induce IgA secretion from naïve B cells. J Immunol 171:3684-3690.

Scandella E, Men Y, Legler DF, Gillessen S, Prikler L, Ludewig B, et al. 2004. CCL19/CCL21-triggered signal transduction and migration of dendritic cells requires prostaglandin E2. Blood 103:1595-1601.

Schnurr M, Then F, Galambos P, Scholz C, Siegmund B, Endres S, et al. 2001 Extracellular ATP and TNF-α synergize in the activation and maturation of human dendritic cells. J Immunol 165: 4704-4709.

Schnurr M, Toy T, Stoitzner P, Cameron P, Shin A, Beecroft T, et al. 2003. ATP gradients inhibit the migratory capacity of specific human dendritic cell types: implications for P2Y11 receptor signaling. Blood 102:613-620.

Shigemoto-Mogami Y, Koizumi S, Tsuda M, Ohsawa K, Kohsaka S, Inoue, K. 2001. Mechanisms underlying extracellular ATP-evoked interleukin-6 release in mouse microglial cell line, MG-5. J Neurochem 78:1339-1349.

Silbergeld EK, Silva IA, Nyland JF. 2005. Mercury and autoimmunity: implications for occupational and environmental health. Toxicol Appl Pharmacol 207:S282-S292.

Steinman RM, Bonifaz L, Fujii S, Liu K, Bonnyay D, Yamazaki S, et al. 2005. The innate functions of dendritic cells in peripheral lymphoid tissues. Adv Exp Med Biol 560: 83-97.

Valk E, Zahn S, Knop J, Becker D. 2002. JAK/STAT pathways are not involved in the direct activation of antigen-presenting cells by contact sensitizers. Arch Dermatol Res 294:163-167. Epub 2002 Jun 01.

Voss AA, Lango J, Ernst-Russell M, Morin D, Pessah IN. 2004. Identification of hyperreactive cysteines within ryanodine receptor type 1 by mass spectrometry. J Biol Chem 279:34514-34520.

Zhang J. 1984. Clinical observations in ethyl mercury chloride poisoning. A J Indust Med 5:251-258.

Zimanyi I, Buck E, Abramson JJ, Mack MM, Pessah IN 1992. Ryanodine induces persistent inactivation of the Ca2+ release channel from skeletal muscle sarcoplasmic reticulum. Mol Pharmacol 42:1049-1057.

Table 1. Mean signal intensities of calcium channel and selected immune marker gene expression in immature and mature bone marrow-derived DCs from C57BL/6 mice. DCs were cultured without 2-Me at 5% O_2. Data are from three independent DC cultures.

	IMMATURE DC	**MATURE DC**
Gene product, (accession#)	Signal[a] , Call[b]	Signal, Call
	MEAN SIGNAL INTENSITIES	
Ryanodine receptor type 1, (gb:X83932.1)	99, 360, 178 (P)	59, 114, 107 (P)
Ryanodine receptor type 2, (gb: NM_023868.1)	8, 2, 2 (A)	18, 6, 2 (A)
Ryanodine receptor type 3, (gb: AV238793)	13, 3, 13 (A)	34, 75, 48 (P)
Inositol 1,4,5-trisphosphate receptor 1, (gb:NM_010585.1)	77, 148, 147 (P)	183, 178, 181 (P)
Inositol 1,4,5-trisphosphate receptor 2, (gb:NM_019923.1)	31, 23, 32 (A)	50, 27, 46 (A)
Inositol 1,4,5-trisphosphate receptor 3, (gb:NM_080553.1)	116, 128, 115 (P)	87, 95, 68 (P)
MHC class II H2-IA$_\beta$, (gb:M15848.1)	2493, 4467, 3727 (P)	1454, 2340, 1775 (P)
CD86 (gb:NM_019388.1)	167, 399, 596 (P)	398, 721, 669 (P)
GADPH, (gb:NM_008084.1)	11241, 4761, 4547 (P)	11126, 4635, 5186 (P)

a= Relative RNA expression, individual values are given for 3 assays. The first value is from hybridization to a Affymetrix mouse 430A GeneChip array (Affymetrix Inc.), the second and third values are from hybridization to a 430 2.0 GeneChip array.

b= (A)= transcript absent; (P)= transcript present. GADPH= glyceraldehyde-3-phosphate dehydrogenase.

FIGURE LEGENDS

Figure 1. DCs express IP_3R and RyR Ca^{2+} channels. IDCs were dual labeled with anti-IP_3R1 (A) and anti-RyR Abs (C). Cells stained with anti- IP_3R1 Ab plus blocking peptide (B) and fluorescent second step Ab (D). Nuclei were counterstained with 7AAD. 100X original magnification. Merged images of RyR1 and IP_3R (pan anti IP_3R Ab) immunostaining in IDCs (E); RyR1 and 7AAD nuclear staining (F). Images were acquired at 100x with 2.5x digital magnification. 40x magnification of IDCs (G) and MDCs (H) stained for RyR. Scale bars indicate 10 μm.

Figure 2. IDCs respond to caffeine and ATP. IDCs were loaded with fluo-4 or fura-2 as described in methods. IDCs that responded to caffeine (40 mM) also responded to 20 μM ATP (A). Cells that failed to respond to ATP also did not respond to caffeine (not shown). The ATP response magnitude (averaged trace of 20 cells shown) was dose dependent (B). An independent experiment was performed for panels (A) and (B).

Figure 3. Dose-response survival curves and IC_{50} values for IDCs and MDCs treated 20 h with thimerosal (THI), ethylmercuric chloride (EtHgCl), or thiosalicylic acid (TSA) (A, B). Survival curves plotting percent propidium iodide (PI) negative cells v. medium control (as 100 percent) for IDC and MDC. TdT DNA strand labeling and confocal microscopy of IDCs treated with medium (C), 500 nM TSA (D), or 500 nM THI (E) for 20 h. Nuclei with strand breakage stain green; all nuclei are counterstained red with propidium iodide. Note the small and round apoptotic morphology of the thimerosal treated nuclei compared to controls. 40X original magnification. Scale bars indicate 10

μm. THI and EtHgCl inhibit [^{3}H]Ry binding to RyR1 high affinity sites (F). Receptor binding analysis was performed as described in Methods. IC_{10}, IC_{20}, and IC_{50} values were determined by non-linear curve fitting. TSA had no effect at the highest concentration tested. Data shown are the average of two independent experiments.

Figure 4. Ca^{2+} transients elicited in IDCs by ATP before and after 20 min exposure (bars underneath traces) to buffer, 50 nM THI, or 100 nM THI. DC were given 20 μM ATP (5 s, first downward arrow) 1 min after the start of trace recording. The cells were challenged a second time with ATP and traces recorded 8 min. Thin horizontal line indicates the initial baseline. $R_{340/380}$ ratiometric data was acquired every 2 s. Traces are the mean ± SE and are representative of two experiments.

Figure 5. Ryanodine and THI functionally uncouple IP_3R1 and RyR1 in IDCs. (A) Shows Ca^{2+} transients elicited by ATP (20 μM, 5 s) applied to IDCs that were pre-incubated either with buffer (first trace from top), 100 μM ryanodine (Ry for 4 h; second trace); 100 nM THI (5 min; third trace), or 100 μM Ry (4 h) + 100 nM THI (5 min) (fourth trace). Traces are mean responses ± SE and represent one of two experiments. Ry nor THI singly or combined alter time to peak response towards 20 μM ATP (B). However Ry and/or THI significantly shorten the recovery time to baseline (C), persistently elevated the recovery baseline for resting [Ca^{2+}] (D), and recruited more ATP-responsive DC (E). Panels B-E are statistics (mean ± SE) derived from the cells in (A). Results were replicated in three independent experiments.* $p<0.05$; **$p<0.01$

Figure 6. THI suppression or exacerbation of ATP mediated IL-6 secretion from IDCs is dependent on the ATP dose. IL-6 accumulation induced by 0.2 μM ATP is suppressed by 100 nM THI (A). Kinetics of IL-6 secretion induced by 2 μM or 20 μM ATP is enhanced by 100 nM THI (B, C). DCs were pretreated with THI or TSA as in (A). Data are means of quadruplicates ± SE. An independent cell culture was used for each graph in panels 6A-C. *p>0.05

Figure 7. Model of how THI and Ry uncouple regulation of Ca^{2+} transients elicited by ATP in IDCs. Solid line depicts a typical Ca^{2+} transient triggered by ATP in naïve IDCs (Figure 4A). Under these conditions IP_3R1 and RyR1 are functionally coupled. Dashed line depicts observed changes in the ATP-triggered Ca^{2+} transient after preincubation with THI (100 nM, 5 min) or RyR1 channel block (100 μM Ry, 4 h). The rising phase of the transient (Phase 1) remains unchanged by either THI or Ry treatments (singly or combined) and is generated by IP_3R activation. Transient termination is significantly faster after RyR1 modification by THI or Ry (singly or combined) (Phase 2). Modified RyR1, IP_3R1 and/or Ca^{2+} entry may become 'leaky' resulting in a persistent elevation in resting Ca^{2+} (Phase 3). Modification of RyR1 conformation by either THI or Ry is sufficient to uncouple Phase 2 and 3 (see text for details).

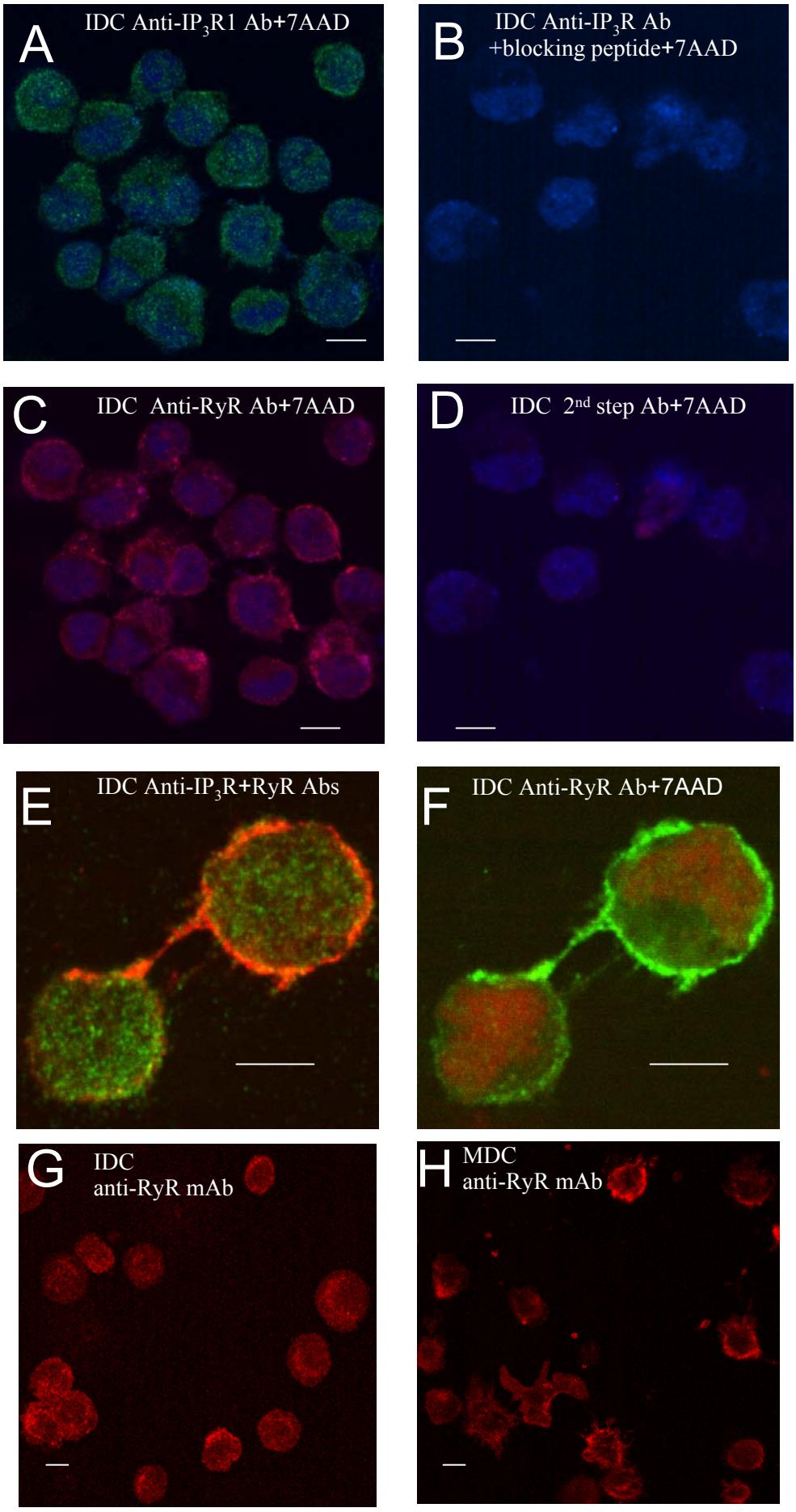

Figure 1
Goth, et al

Figure 2
Goth, et al

A

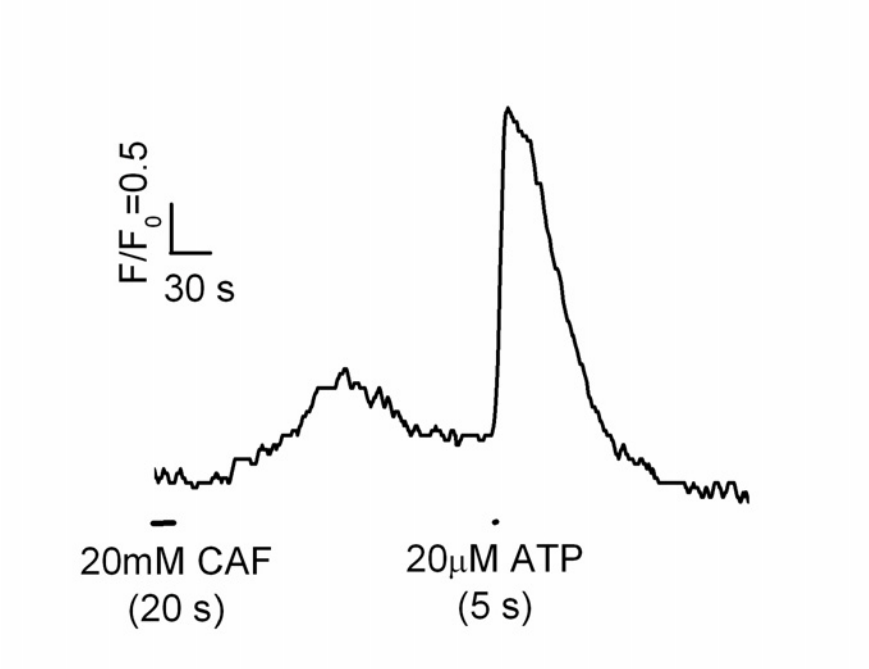

B

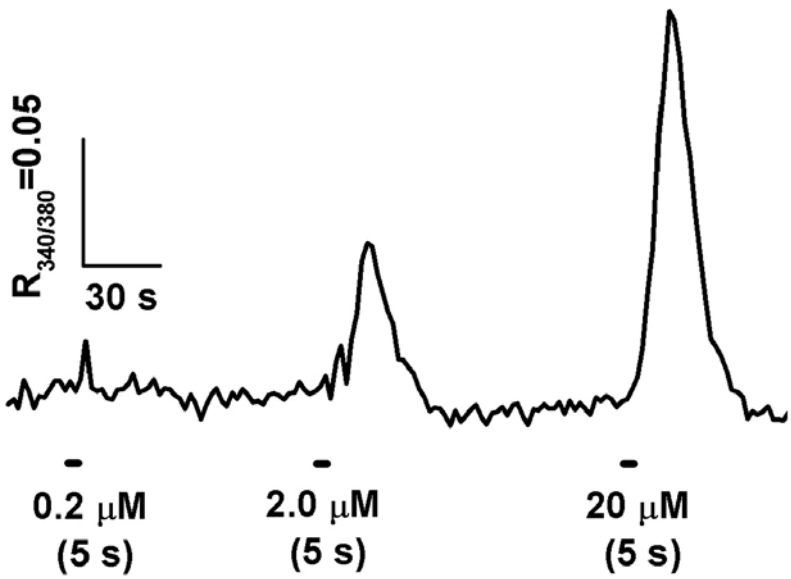

Figure 3, Goth et al.

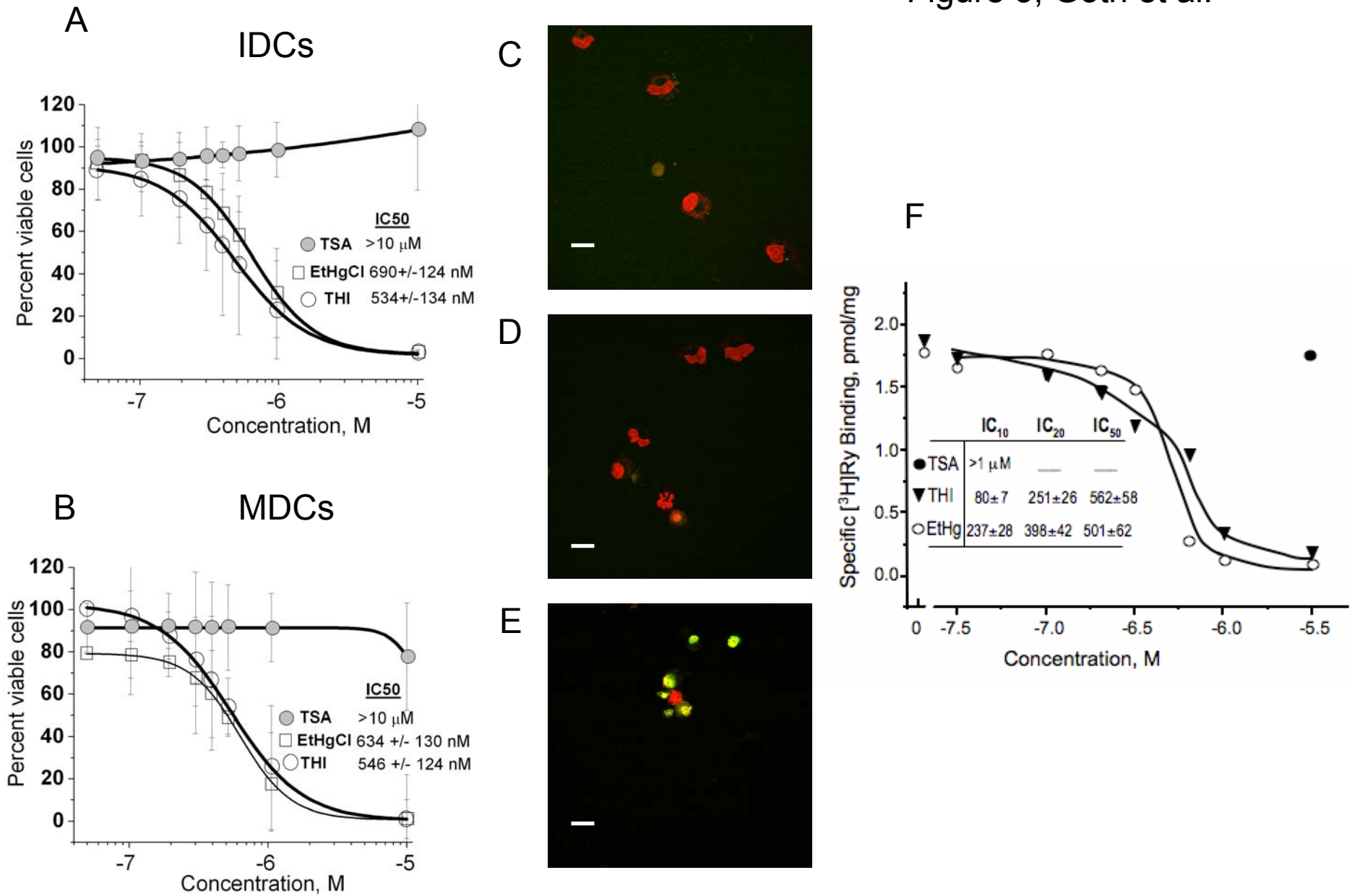

Figure 4 Goth et al

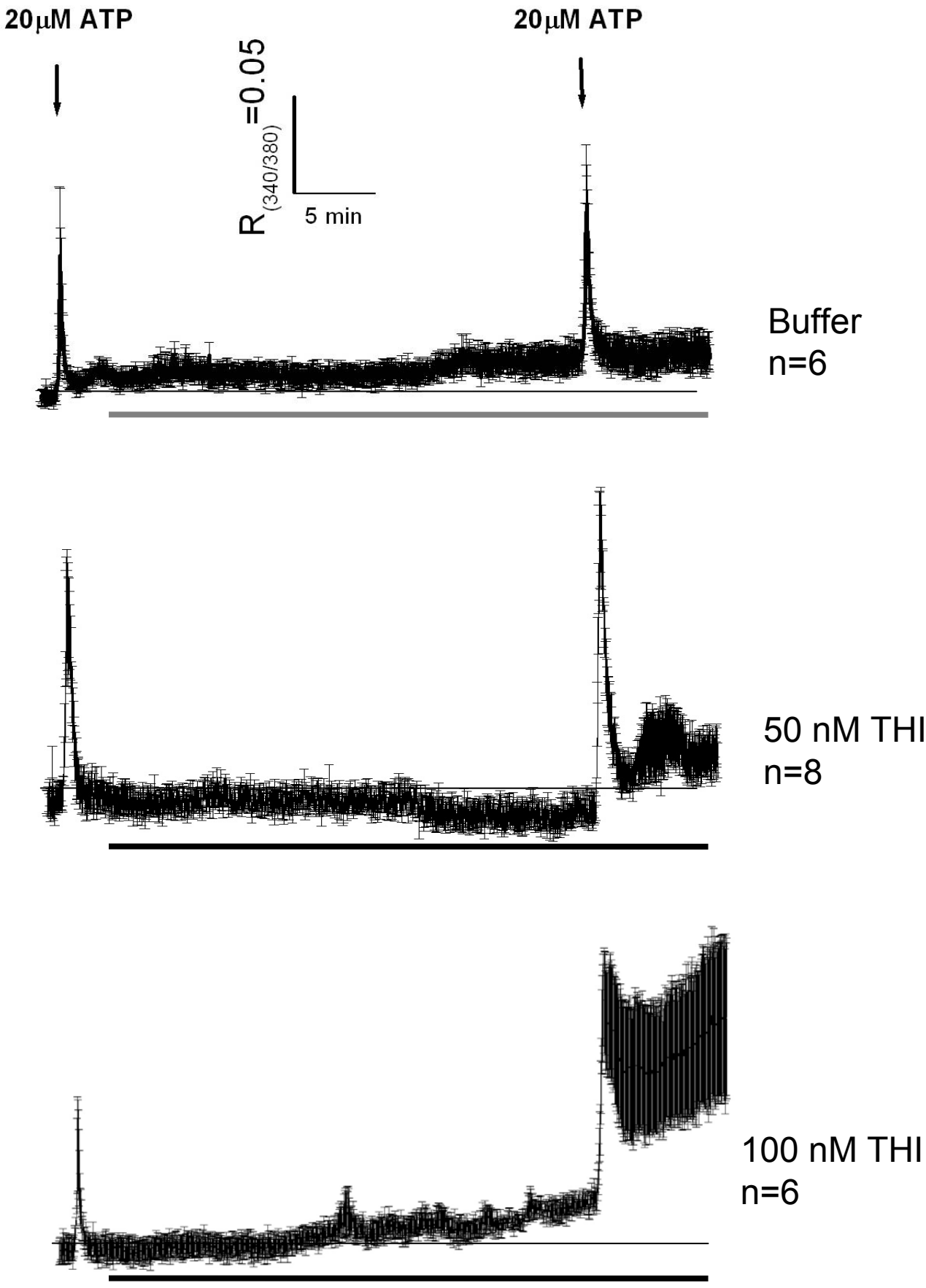

Figure 5 Goth et al

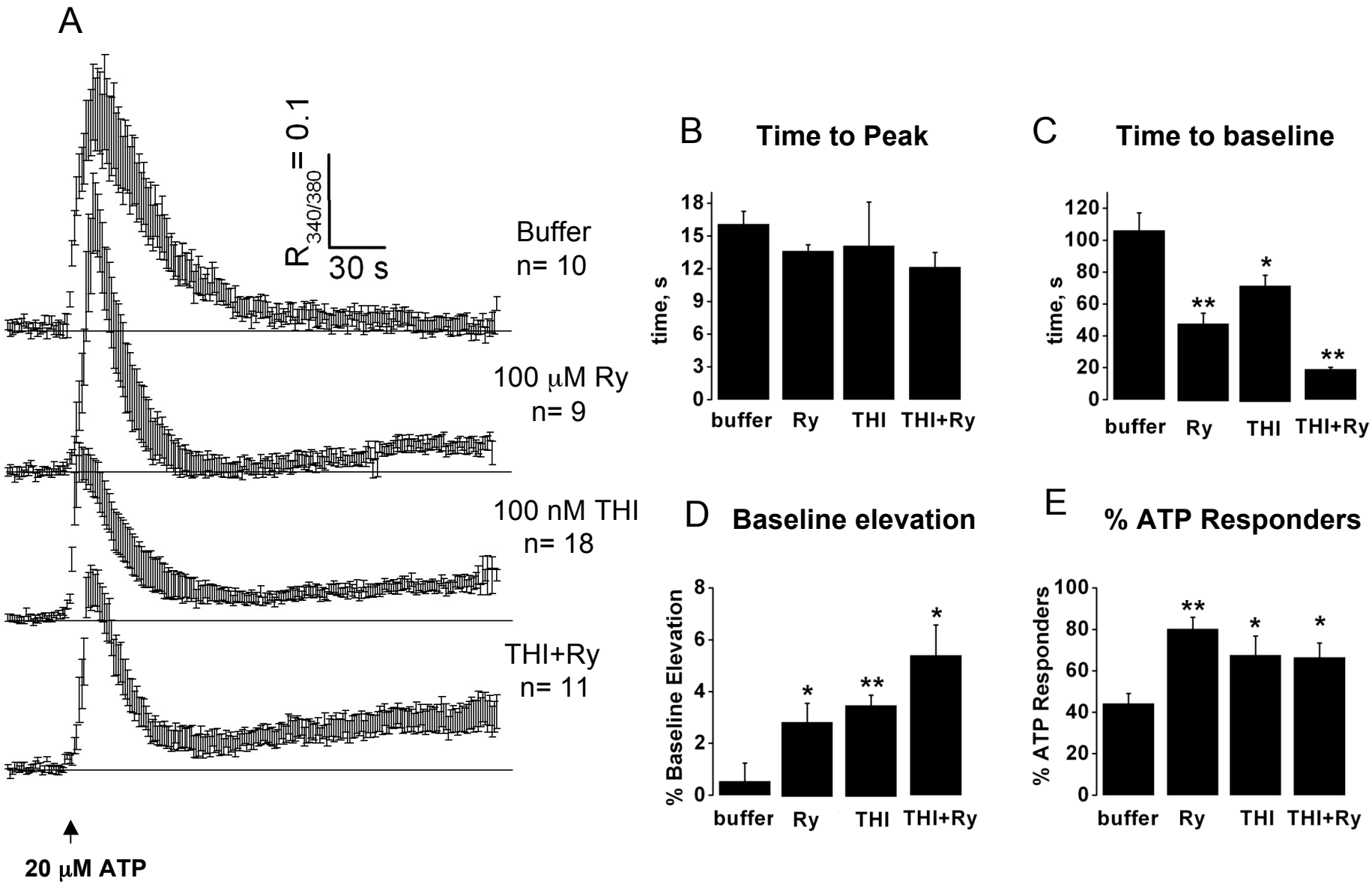

Figure 6 Goth, et al

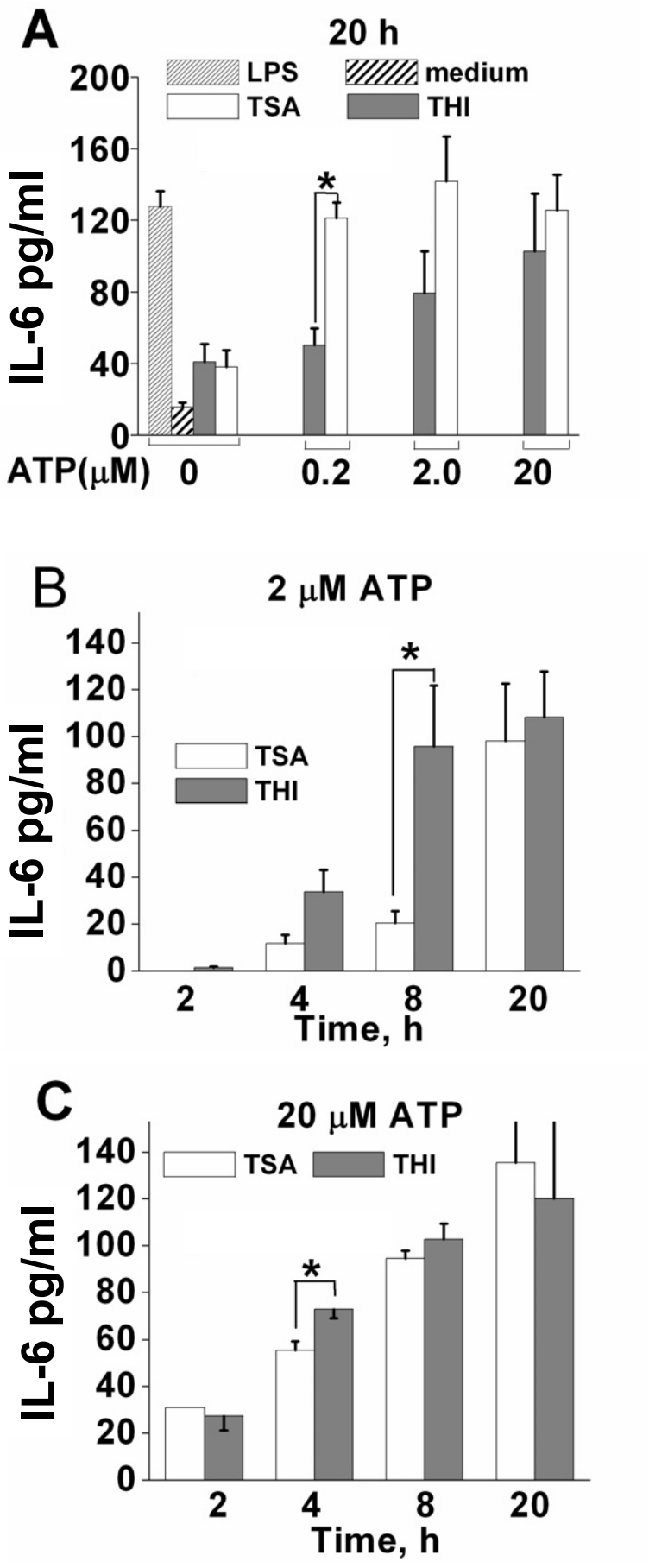

Figure 7 Goth, et al